Data-Efficient Design of High-Entropy Oxygen Carriers for Chemical Looping Using Active Learning

ACS MATERIALS Au
AN OPEN ACCESS JOURNAL OF THE AMERICAN CHEMICAL SOCIETY

pubs.acs.org/materialsau
Letter

Data-Efficient Design of High-Entropy Oxygen Carriers for Chemical Looping Using Active Learning

Published as part of ACS Materials Au special issue "Integrating Machine Learning in Modelling Catalysis at the Nanoscale".

Joakim Brorsson, Henrik Klein Moberg, Joel Hildingsson, Jonatan Gastaldi, Tobias Mattisson, and Anders Hellman*

Cite This: ACS Mater. Au 2026, 6, 319–326

ABSTRACT: High-entropy materials, first demonstrated in metallic alloys and later extended to oxides and other systems, unlock a vast compositional space with properties suited for catalysis, energy, and structural materials. However, the high compositional complexity makes systematic exploration challenging, and only a small portion of the design space has been studied. To address this, we introduce an active learning strategy that integrates predictive modeling, uncertainty estimation, and iterative sampling to efficiently navigate embedded compositional material spaces. This approach continuously learns from previous evaluations, focusing subsequent searches on the most promising regions while reducing both time and data requirements. We demonstrate this methodology in the search for high-entropy oxygen carriers for chemical looping, where it rapidly accelerates discovery and identifies promising candidates more effectively than conventional trial-and-error or grid-search approaches. Importantly, this strategy is general and well-suited to exploring the vast space of multicomponent materials.

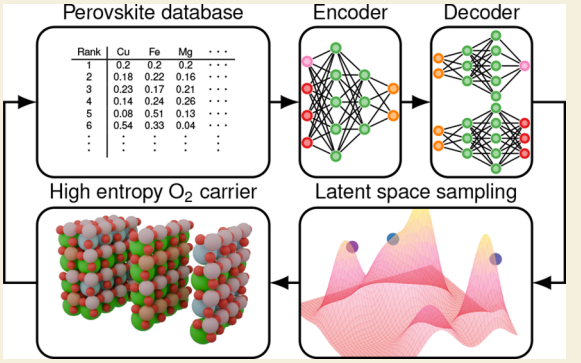

KEYWORDS: *materials discovery, active learning, oxygen carriers, chemical looping, high entropy oxides, machine learning potentials, first-principles*

High entropy materials (HEMs) are, by definition, made up of five or more elements.[1,2] The resulting compositional space combined with entropy-stabilized phases enables a shift from "using the material you have" to "engineering the material you need".[3] By virtue of simple combinatorics, the compositional space of such complex materials can be enormous,[4] making traditional approaches to materials discovery ineffective, and calls for more advanced strategies to accelerate the process. This is especially important for materials that enable next-generation energy conversion technologies, which must be developed rapidly to address environmental and climate challenges.[5] Recently, various machine learning (ML) methods have been utilized, allowing, e.g., the discovery of up to several hundred thousand stable compounds by scanning millions or billions of material candidates.[6−8] While these efforts mark major progress, they demand substantial computational resources and training data, and even such large-scale searches still probe only a minute fraction of the enormous compositional space of HEMs. In response to this challenge, Rao et al.[9] introduced an active learning (AL) strategy, which requires only sparse data for training, to explore high entropy Invar alloys, revealing several candidates exhibiting both thermal stability and low thermal expansion coefficients. Drawing inspiration from this work, the present study aims to demonstrate how AL can be generalized to accelerate the search for any type of HEM. Central to this generalization is the use of adaptable material property functions, e.g., stability, phase transitions between reduced and oxidized states, configurational entropy, or elemental abundance, which enable steering the AL cycle toward the most relevant regions of the design space.

As a proof of concept, we apply the approach to identify next-generation high entropy oxides (HEOs) to be used in chemical looping (CL), a process for efficient fuel conversion which can be applied to combustion, gasification, and reforming. CL has been suggested as a breakthrough technology for achieving carbon capture and storage at low

Received: November 24, 2025
Revised: January 11, 2026
Accepted: January 12, 2026
Published: January 22, 2026

https://doi.org/10.1021/acsmaterialsau.5c00230
ACS Mater. Au 2026, 6, 319–326

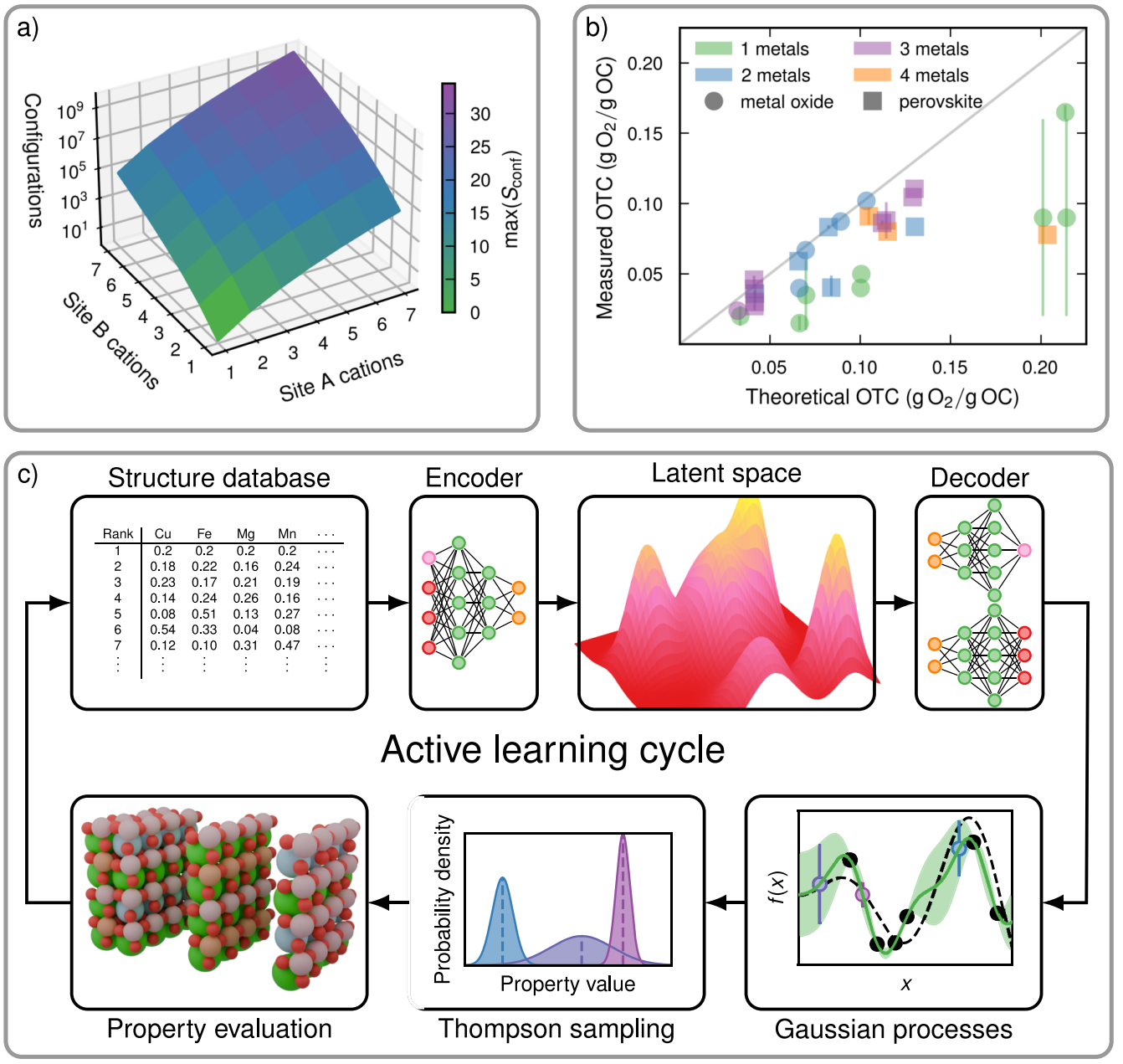

Rank	Cu	Fe	Mg	Mn	⋯
1	0.2	0.2	0.2	0.2	⋯
2	0.18	0.22	0.16	0.24	⋯
3	0.23	0.17	0.21	0.19	⋯
4	0.14	0.24	0.26	0.16	⋯
5	0.08	0.51	0.13	0.27	⋯
6	0.54	0.33	0.04	0.08	⋯
7	0.12	0.10	0.31	0.47	⋯
⋮	⋮	⋮	⋮	⋮	⋮

Figure 1. (a) Number of possible configurations together with the maximum configurational entropy for an 80-atom ABO_3 perovskite supercell plotted against the number of different cations that share the A and B sites. (b) Measured versus theoretical OTCs reported for various oxides (circles) and perovskites (squares) featuring one (green), two (blue), three (purple), or four (orange) distinct metallic elements (see Table S1).[20−26,31−52] (c) Schematic illustration of the AL cycle, in which the first step is to encode a database of compositions and target properties into a continuous latent space via a WAE-GMM model. Then Thompson sampling is used to select candidates, based on estimated property values and uncertainties obtained from GP. Following validation, with CHGNET, the results, which include updated property values, are fed back into the database, enabling iterative learning and refinement.

cost.[10] The core idea is to utilize a solid oxygen carrier (OC), typically a metal oxide, to separate the conversion process into two distinct chambers: one for air and one for fuel[11−13] (see Figure S1). As it mechanically circulates between these reactors, the OC is oxidized in the air reactor and reduced in the fuel reactor. The OC particles must have redox energetics compatible with the process, enabling oxygen uptake in the air reactor and release in the fuel reactor. Further, the OCs must have sufficient oxygen transfer capacities (OTCs) to convert the fuel to the desired products. The initial focus was on monometallic oxides based on transition metals Ni, Fe, Cu, Mn, and Co.[10] To overcome restrictions with respect to stability and reactivity, in the past decade, a number of higher-order systems, including cubic HEOs and ABO_3-type perovskites, have been studied by several different groups, leading to the identification of some promising candidates.[14,15] Still, it should be emphasized that CL is still at a relatively low technical readiness level, with most experiments performed in small pilot units, with OC stability and reactivity being major barriers for up-scaling. So far, most OC development has been based on simple thermodynamics and "trial-and-error" approaches, strategies that become

https://doi.org/10.1021/acsmaterialsau.5c00230
ACS Mater. Au 2026, 6, 319−326

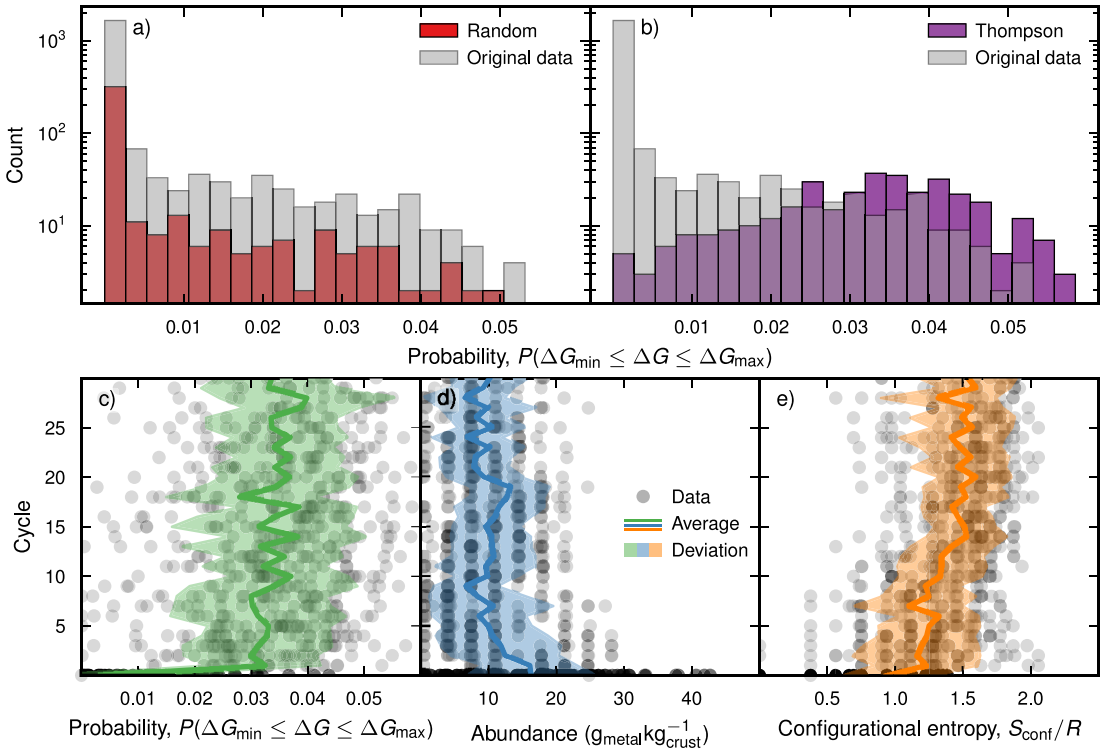

Figure 2. Diagrams with counts of the number of unique candidates with a given value on the target property, i.e., the probability of being suitable as an OC for dry reforming using CL, for the new materials identified when using random (a) and Thompson (b) sampling. Furthermore, the probability (c), average abundance of the metallic elements in the earth's crust (d), and configurational entropy, i.e., S_{conf}/R, (e) are displayed for the original (gray circles) and added (purple circles) data when using the latter method. Here, the averages (solid line) and standard deviations (filled curve) are also indicated.

unmanageable as the compositional space increases. Although there have been some high-throughput studies for the discovery of new OC materials,[13,16,17] no studies using AL approaches have been published. Hence, it is of central importance to find efficient methods to accelerate the development of higher-order OCs.

The focus in this study is ABO_3 perovskites, a class of materials that have been shown to be viable as OCs, and which can also be doped in order to achieve high-entropy configurations. Here, A represents a larger and B a smaller cation that are coordinated by 6 and 12 oxygen atoms, respectively. The stable crystal structure is also advantageous in CL applications since it allows oxygen transfer to occur via the formation of defects rather than phase transformations, in contrast to simple monometallic systems.[18] Even so, the introduction of additional elements, on either or both sublattices, causes an exponential increase in possible configurations (Figure 1a), compromising the tractability after just a few additions. This is accompanied by a steady rise in the maximum configurational entropy, underscoring the high-entropy character attained via cation mixing on multiple sublattices (Figure 1a). A comparison of literature-reported estimated and experimental OTC values shows good agreement across a range of compositional complexities, as demonstrated by comparing oxides and perovskites with one to four distinct cations (see Figure 1b and Table S1). Notably, multicomponent perovskite OCs (e.g., quaternary oxides) show similar or better performance than simpler single- or binary-metal oxides. Hence, there are compelling reasons to construct efficient AL strategies to identify high-entropy OCs. Still, caution should be emphasized when comparing computational predictions with experimental data, as there exist many sources of error in both cases. In the present study, it has been necessary to balance speed and accuracy in order to test and optimize AL framework, since this requires sizable samples to be produced over multiple cycles without expending unreasonable time and computational resources. Consequently, a conservative limit has been used for the non-stoichiometry, i.e., $\delta \leq 0.5$ in ABO_3, which not only agrees well with measurements for $CaMnO_3$[19] but also, more importantly, ensures compliance with the study of Wang et al.[16] While δ values as high as ∼2.0 have been reported for some chemistries, evidence that the perovskite structure is retained after the reduction is seldom provided;[20−24] in fact this has been proven not to be the case for, e.g., $MgMnO_{3-\delta}$ and $CaMn_{0.9}Mg_{0.1}O_{3-\delta}$.[25,26] As the goal of the present study is to identify the best candidates via ranking, systematic errors, such as the assumption of a too low maximum for δ, will have a limited impact on the final results.

The AL model (see Figure 1c) consists of a Wasserstein autoencoder (WAE). Specifically, its task is to learn the latent representation of the data, which is modeled using a Gaussian mixture model (GMM) to ensure that the corresponding space is continuous, tractable, and chemically informative (see Figure S2). At this stage, sampling is performed within the latter to identify points that are proximal to the original data manifold and, thus, likely to represent chemically valid compositions. Gaussian processes (GP) is subsequently applied to assess uncertainty and facilitate the selection of promising compositions via Thompson sampling,[27] thereby balancing exploration and exploitation. Candidates are ranked according to their predicted target properties, and subsequently evaluated with

https://doi.org/10.1021/acsmaterialsau.5c00230
ACS Mater. Au 2026, 6, 319−326

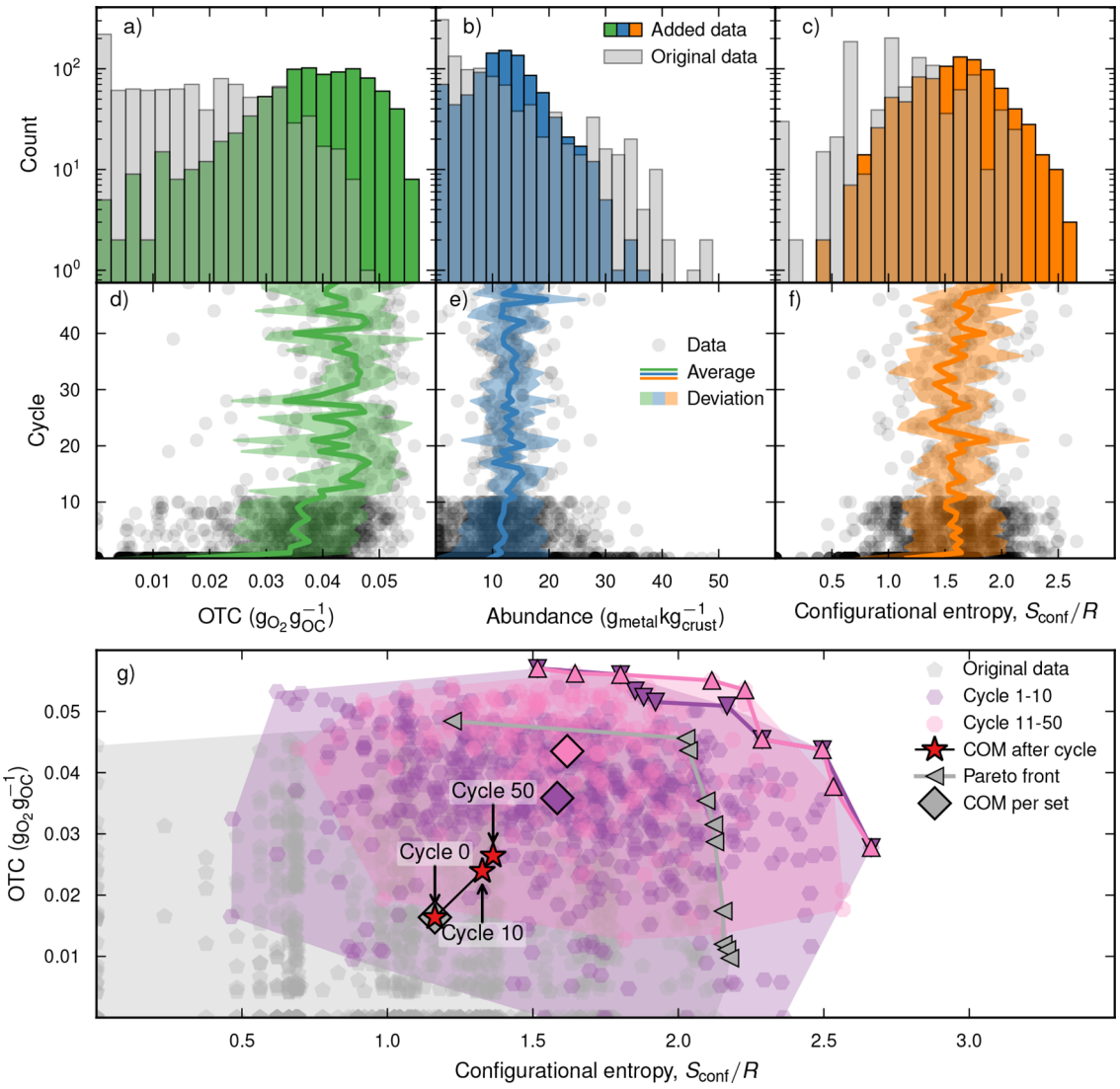

Figure 3. Diagrams with the computationally verified OTC (a,d); average abundance of the metallic elements in the earth's crust (b,e); and configurational entropy, S_{conf}/R, (c,f) versus counts of the number of unique candidates (a−c) and those added in each cycle (d−f) as well as a Pareto plot (g). Specifically, this includes data from the original training set (gray circles) together with cycles 1−10 (purple circles) and 11−50 (pink circles). In the second row, averages (solid line) and standard deviations (filled curve) are also shown. Additionally, the Pareto fronts (triangles) as well as the center-of-mass for the individual sets (diamonds) and the accumulated data up to a certain cycle (red stars) are displayed in the last panel.

respect to their thermodynamic properties (see Figure S3) using CHGNET,[28] a state-of-the-art machine learning interatomic potential (MLIP) trained on 1.6 million entries from the Materials Project.[29,30] Although first-principles or experimental validation could, in principle, be employed, CHGNET was chosen to enable faster iteration and screening. Finally, the evaluated candidates—with updated target properties—are incorporated into the database. Through iterative cycles of model training, probabilistic candidate generation, and property evaluation, this AL strategy rapidly pinpoints promising high entropy oxygen carriers (HEOCs) from a myriad of possible ABO_3 configurations.

To highlight the AL strategy and its data efficiency, we first focus on the prediction of HEOCs based on ABO_3 perovskites for reforming via CL for production of H_2 and CO_2. Here, a limited training data set from the study by Wang et al.[16] was utilized. In their study, the design space of perovskite oxides was systematically expanded by taking $SrFeO_3$ as a parent structure and exploring extensive A- and B-site substitutions through high-throughput density functional theory (DFT) calculations. This substitution strategy yielded a diverse data set of approximately 2400 compositions, several of which exhibited superior redox behavior compared to the baseline $SrFeO_3$.

We randomly select only 10%—a limited collection of ∼240 candidates—as our initial database. Additionally, the entries in this database are updated with the probability of the candidate being suitable for dry reforming using CL (see Methods section), which will be the target property optimized during the cycles. Candidates were filtered for charge neutrality and Goldschmidt tolerance in each cycle. After five parallel runs of 30 cycles each, approximately 200 new OCs had been identified, which demonstrated the strong data efficiency. Compared to a purely random or unguided strategy (see Figure 2a), the histogram of discovered materials from the WAE-GMM model with Thompson sampling is skewed

https://doi.org/10.1021/acsmaterialsau.5c00230
ACS Mater. Au 2026, 6, 319−326

toward the upper end of the probability range, indicating that it identifies significantly more high-probability OCs (see Figure 2b). This underscores the efficacy of AL in navigating the compositional space. Further analysis of the candidates selected by this approach shows that the top-ranking compositions (those with the best predicted dry reforming capability) tend to exhibit a high compositional complexity, often containing five or more different cations. This is evident in the all-candidate averages per cycle, which show a steady increase in configurational entropy, decreases in mean metal abundance, and higher probability with each iteration (Figure 2c–e). In other words, the algorithm progressively shifts toward more compositionally diverse (but less common) regions of the search space in the pursuit of higher predicted performance materials.

The results in Figure 2 clearly demonstrate the advantages of AL strategies over traditional methods, i.e., "trial-and-error" or grid search. Even so, the probability-based measure that we used as a target value, while useful for guiding experiments, is difficult to compare with measurements. To demonstrate that the methodology is equally effective for directly measurable properties, we also addressed the problem of identifying HEOCs with a maximum of OTC under chemical looping combustion (CLC) conditions. In this case, it is necessary to leverage two additional properties: the configurational entropy and the Bartel tolerance factor (τ). The former should, more precisely, not exceed 1.5R in order to satisfy the HEM criteria, while the latter, which predicts the stability and synthesizability of ABO_3 perovskite structures, was strictly required to be lower than 4.18—candidates with a higher value were filtered out.

In order to achieve more accurate OTC estimates, the representative special quasi-random structures (SQSs) were based on larger (80-atom) supercells and covered multiple crystal symmetries, i.e., orthorhombic, cubic, and brownmillerite. In addition, a broader training data set was constructed, to obtain a better starting point for the model, by generating 1815 random ABO_3 configurations, of which 1066 remained after those with low configurational entropy and high Bartel tolerance had been filtered out. The same AL framework was employed, although the design space was expanded by many orders of magnitude owing to the larger supercell. To enable a broader search, five independent runs of 10 cycles each were carried out using identical training sets but different random seeds. The resulting candidates were merged into a single data set, which was subsequently advanced through 40 additional cycles (see Figure 3).

It is important to note that the AL algorithm was optimized solely with respect to the OTC while still fulfilling the criteria for the different CL processes. Nevertheless, the training procedure led to the selection of structures with both lighter elements and increased configurational entropy compared to the initial data set (see Figure 3a–f). This demonstrates that the WAE-GMM model combined with Thompson sampling is highly effective at identifying promising candidates. Notably, top-performing materials such as $Ca_{13}CoMgMn_9Ti_5Y_3O_{48}$, $Ca_{11}Mg_3Mn_8Ti_5Y_5O_{48}$, and $Ca_{11}FeMg_3Mn_8Ti_4Y_5O_{48}$ achieved OTC scores of $0.0570\ g_{O_2}g_{OC}^{-1}$, $0.0562\ g_{O_2}g_{OC}^{-1}$, and $0.0560g_{O_2}g_{OC}^{-1}$, respectively, and interestingly, all include Ca and Mn—elements well-known for their strong oxygen-carrying capabilities. The fact that the Pareto front successively expands with respect to both the OTC, as obtained from the first-principles calculations, and configurational entropy provides further evidence of the strength of AL (see Figure 3g). Indeed, the majority of the added points, after 10 cycles, have a configurational entropy $S_{conf} \geq 1.5R$ and an OTC of at least $0.03g_{O_2}g_{OC}^{-1}$. Moreover, this trend grows stronger with the number of cycles.

Taken together, our results illustrate that AL provides an efficient and robust framework for discovering new materials, especially in systems in which the configurational space is vast. We have not only discovered many promising OCs for dry reforming and CLC but also shown how the generative model improves steadily over the training cycles. Thanks to its inherent flexibility, this approach can be readily extended to other material classes as well as applications and adapted by, e.g., replacing or combining ab initio calculations with experiments. We therefore envision that AL strategies that integrate WAE-GMM with Thompson sampling will become increasingly important in both applied and fundamental materials science, thereby advancing the design of multi-component oxides for sustainable energy technologies.

METHOD

In the sections that follow, we provide a condensed overview of the methodology employed in this study; a more detailed description can be found in reference 53.

Active Learning

We use AL to refine a surrogate model, which predicts material properties and estimates the associated uncertainty, in a way that balances exploration and exploitation (for more details, see Note S1). An acquisition function is applied for querying in each round, whereafter the surrogate is updated. Here, Thompson sampling is utilized, which is designed to sample the posterior of the model based on the identification of promising or informative points because of its simplicity and effectiveness.[27,54] To generate candidates, we have, more precisely, chosen to couple a WAE[55] with a GMM. The rationale for this choice is to take advantage of the former architecture and the adaptable encoding offered by the latter. In this way, we obtain a flexible yet structured latent representation with the capacity to capture the intricacies of compositional relationships. The trained WAE can thus be conditioned to sample compositions, in a controlled manner, that are not only chemically reasonable but also likely to have desirable target properties.

Structure Generation and Filtering

Similarly to Wang et al.,[16] the training data used for testing the AL methodology for CL dry reforming consisted of 2401 cubic 40 atom $Sr_{1-x}A_xFe_{1-y}B_yO_{3-\delta}$ supercells, with Sr and Fe partially substituted by A = Ca, K, Y, Ba, La, Sm and B = Co, Cu, Mn, Mg, Ni, Ti, respectively. In particular, this meant that x and y ranged from 0 to 1 in steps of 0.0125. The same applies to the oxygen nonstoichiometry δ, except that the upper limit was 0.5 instead. In addition, the brownmillerite structure, $Sr_{2-2x}A_{2x}Fe_{2-2y}B_{2y}O_5$, was included for temperatures below 800 °C, to account for a possible decomposition when $\delta \rightarrow 0.5$. When attempting to find HEOCs for CLC, however, 1815 random ABO_3 80 atom supercells were generated to form the original training data. This meant that the step size in the oxygen nonstoichiometry was reduced to 0.0625. In addition, orthorhombic as well as cubic symmetries were considered together with the brownmillerite structure. Hence, the number of distinct SQSs evaluated for each composition was increased

https://doi.org/10.1021/acsmaterialsau.5c00230
ACS Mater. Au 2026, 6, 319–326

from 7 to 19, compared with the aforementioned verification study. Note that the ground state structures of $SrFeO_3$ and $Sr_2Fe_2BO_5$ in the Materials Project[29,30] were consistently used as starting points regardless of the actual composition.

In agreement with Wang et al.,[16] unstable compositions were excluded according to charge balance (Δq_e) together with a tolerance factor. Specifically, all initial training structures, as well as the proposed CLC candidates during the AL cycles, were evaluated based on the Bartel tolerance

$$\tau = \frac{\overline{r}_X}{\overline{r}_B} - \overline{n}_A\left(\overline{n}_A - \frac{\overline{r}_A/\overline{r}_B}{\ln(\overline{r}_A/\overline{r}_B)}\right) \tag{1}$$

where $\overline{r}_i$ and $\overline{n}_i$ are the average radius and oxidation state on site $i \in \{A, B, X\}$ in ABX_3; presently X is occupied by oxygen atoms and vacancies.[56] When considering CL dry reforming, enforcing $\Delta q_e = 0$ and $\tau \leq 4.3$ narrowed the size of the predefined data set from 2401 to 2069. Also note that the Goldschmidt tolerance factor

$$\tau = \frac{\overline{r}_A + \overline{r}_X}{\sqrt{2}(\overline{r}_B + \overline{r}_X)} \tag{2}$$

was used to assess the stability of the added compositions in this case. For CLC, meanwhile, both charge neutrality and a Bartel tolerance of $\tau \leq 4.18$ were consistently required, leaving only 1066 of the 1815 original training structures.

Property Estimates

The universal CHGNet MLIPs[28] was utilized for the force and energy calculations. In addition, the ASE implementation[57] of the Broyden–Fletcher–Goldfarb–Shanno (BFGS) algorithm was used for all structural relaxations, thereby ensuring that the interatomic forces did not exceed 0.001 eV $Å^{-1}$. The lattice heat capacity, on the other hand, was estimated based on the harmonic approximations using the PHONOPY[58] package. More precisely, this involved training force constants using a reciprocal grid with a density of 1000000 $atom^{-1}$ from data obtained by imposing 0.02 Å displacements on specific atoms in supercells with spatial dimensions of at least 12.5 Å.

To assess the probability that a given candidate was suitable for dry reforming, the vacancy formation energies, $\Delta G_{\delta_1\to\delta_2} = G_f^{\delta_2} + \frac{\Delta\delta}{2}\mu_{O_2} - G_f^{\delta_1}$ associated with the reactions

$$Sr_{1-x}A_xFe_{1-y}B_yO_{3-\delta_1} \leftrightharpoons Sr_{1-x}A_xFe_{1-y}B_yO_{3-\delta_2} + \frac{\delta_2-\delta_1}{2}O_2 \tag{3}$$

were compared with energy intervals defined by Wang et al.[16] When calculating Gibbs free energy (G^{δ_i}), the volume contribution $PV_{\delta_i}^{0\ K}$ as well as the discrepancy between the specific heat capacity at constant volume and pressure ($C_V^{\delta_i} \approx C_P^{\delta_i}$) were neglected. Consequently

$$G^{\delta_i}(T) \approx U^{\delta_i}(0\ K) + \int_0^T C_V^{\delta_i}(T')dT' + S^{\delta_i}(0\ K) + \int_0^T \frac{C_V^{\delta_i}(T')}{T'}dT' \tag{4}$$

where $U^{\delta_i}(0\ K)$ and $S^{\delta_i}(0\ K)$ are the internal energy and entropy at 0 K, respectively.

The formation energies were converted into measures of the OC capability by treating the formation energies as mean values (μ) of randomly distributed variables $X \sim \mathcal{N}(\mu, \sigma^2)$ with a standard deviation of $\sigma = 0.4$ eV. The probability that any of the transitions with $\delta_2 - \delta_1 \equiv \Delta\delta = 0.125$ were located within the interval $a < \Delta G_{\delta_1\to\delta_2} \leq b$ is, thus, given by

$$P(a < X \leq b) = F_X(b) - F_X(a) = \frac{1}{\sigma\sqrt{2\pi}} \int_{-\infty}^{x} \exp\left(-\frac{(t-\mu)^2}{2\sigma^2}\right)dt\Big|_{x=a}^{b} \tag{5}$$

where $F_X(x) = F(x; \mu, \sigma)$ is the corresponding cumulative distribution function, while $(a, b) = (1.93\text{ eV}, 2.74\text{ eV})$ at 800 °C and $(a, b) = (1.83\text{ eV}, 2.91\text{ eV})$ at 950 °C. Note that the interpolated formation energies at $\delta \in \{0.0625, 0.1875, 0.3125, 0.4375\}$ were also used in this evaluation.

As a measure of CLC capacity, the OTC was calculated from the difference in the nonstoichiometry ($\Delta\delta = \delta_{red} - \delta_{ox}$) under reducing ($T$ = 1050 °C, $p_{O_2} = 10^{-14}$ atm) and oxidizing (T = 950 °C, p_{O_2} = 0.2 atm) conditions. To be specific, the OTC value is $0.5\Delta\delta M_{O_2}/M_{ABO_3}$ where M_i is the molar mass of compound i.

To obtain a measure of candidate practical viability, the average metal abundance was deemed a better alternative than the material cost due to the inherent volatility in the market prices for individual elements. Specifically, the former was calculated as

$$\overline{X} = \frac{\sum_{Me} n_{Me}X_{Me}}{\sum_{Me} n_{Me}} \tag{6}$$

where n_{Me} is the number of atoms of type Me while X_{Me} is the corresponding abundance in the earth's crust.[59]

■ ASSOCIATED CONTENT

Data Availability Statement

Additional information, including a more elaborate account of the methodology, can be found in ref 53.

Supporting Information

The Supporting Information is available free of charge at https://pubs.acs.org/doi/10.1021/acsmaterialsau.5c00230.

Supporting material that illustrates key aspects of the study, including an overview of the chemical looping combustion process; a schematic of the WAE-based active learning pipeline, as well as a description thereof; and a detailed diagram outlining the procedure used to evaluate the properties of candidate materials (PDF)

■ AUTHOR INFORMATION

Corresponding Author

Anders Hellman − *Department of Physics, Chalmers University of Technology, SE-41296 Gothenburg, Sweden;* orcid.org/0000-0002-1821-159X; Email: anders.hellman@chalmers.se

Authors

Joakim Brorsson − *Department of Physics, Chalmers University of Technology, SE-41296 Gothenburg, Sweden;* orcid.org/0000-0002-7118-4930

Henrik Klein Moberg − *Department of Physics, Chalmers University of Technology, SE-41296 Gothenburg, Sweden*

Joel Hildingsson − *Department of Physics, Chalmers University of Technology, SE-41296 Gothenburg, Sweden*

https://doi.org/10.1021/acsmaterialsau.5c00230
ACS Mater. Au 2026, 6, 319−326

Jonatan Gastaldi − *Department of Space, Earth and Environment, Chalmers University of Technology, SE-41296 Gothenburg, Sweden;* orcid.org/0009-0006-4948-2209
Tobias Mattisson − *Department of Space, Earth and Environment, Chalmers University of Technology, SE-41296 Gothenburg, Sweden;* orcid.org/0000-0003-3942-7434

Complete contact information is available at: https://pubs.acs.org/10.1021/acsmaterialsau.5c00230

Author Contributions

Joakim Brorsson: Conceptualization, Methodology, Investigation, Writing−Original Draft. Henrik Klein Moberg: Methodology, Supervision. Joel Hildingsson: Methodology, Software, Data Curation. Jonatan Gastaldi: Investigation, Resources. Tobias Mattisson: Conceptualization, Supervision. Anders Hellman: Conceptualization, Supervision, Project Administration, Writing−Review & Editing.

Notes

The authors declare no competing financial interest.

■ ACKNOWLEDGMENTS

This work was funded by the Swedish Research Council (2020-03487), and the computations were enabled by resources provided by the Swedish National Infrastructure for Computing (SNIC) at NSC and C3SE, partially funded by the Swedish Research Council through grant agreement nos. NAISS 2023/3-29, NAISS 2023/5-521, NAISS 2024/5-260, NAISS 2024/3-26, and NAISS 2025/5-313.

■ REFERENCES

(1) George, E. P.; Raabe, D.; Ritchie, R. O. High-entropy alloys. *Nature Reviews Materials* **2019**, *4*, 515−534.
(2) Sen, S.; Palabathuni, M.; Ryan, K. M.; Singh, S. High Entropy Oxides: Mapping the Landscape from Fundamentals to Future Vistas. *ACS Energy Letters* **2024**, *9*, 3694−3718.
(3) Bishop-Moser, J.; Miracle, D. Manufacturing High Entropy Alloys: Pathway to Industrial Competitiveness. *Medium*, **2018**.
(4) Aamlid, S. S.; Oudah, M.; Rottler, J.; Hallas, A. M. Understanding the Role of Entropy in High Entropy Oxides. *J. Am. Chem. Soc.* **2023**, *145*, 5991−6006.
(5) IPCC. In *Climate Change 2023: Synthesis Report. Contribution of Working Groups I, II and III to the Sixth Assessment Report of the Intergovernmental Panel on Climate Change*; Team, C. W., Lee, H., Romero, J., Eds.; Intergovernmental Panel on Climate Change (IPCC): Geneva, Switzerland, 2023; pp 35−115.
(6) Merchant, A.; Batzner, S.; Schoenholz, S. S.; Aykol, M.; Cheon, G.; Cubuk, E. D. Scaling deep learning for materials discovery. *Nature* **2023**, *624*, 80−85.
(7) Schmidt, J.; Hoffmann, N.; Wang, H.-C.; Borlido, P.; Carriço, P. J. M. A.; Cerqueira, T. F. T.; Botti, S.; Marques, M. A. L. Machine-Learning-Assisted Determination of the Global Zero-Temperature Phase Diagram of Materials. *Adv. Mater.* **2023**, *35*, 2210788.
(8) Zeni, C.; et al. A generative model for inorganic materials design. *Nature* **2025**, *639*, 624−632.
(9) Rao, Z.; Tung, P.-Y.; Xie, R.; Wei, Y.; Zhang, H.; Ferrari, A.; Klaver, T. P. C.; Körmann, F.; Sukumar, P. T.; Silva, A. K.; et al. Machine learning-enabled high-entropy alloy discovery. *Science* **2022**, *378*, 78−85.
(10) Adanez, J.; Abad, A.; Garcia-Labiano, F.; Gayan, P.; de Diego, L. F. Progress in Chemical-Looping Combustion and Reforming technologies. *Prog. Energy Combust. Sci.* **2012**, *38*, 215−282.
(11) Lyngfelt, A.; Leckner, B.; Mattisson, T. A fluidized-bed combustion process with inherent CO_2 separation; application of chemical-looping combustion. *Chem. Eng. Sci.* **2001**, *56*, 3101−3113.
(12) Zeng, L.; Cheng, Z.; Fan, J.-A.; Gong, J.; Fan, L.-S. Metal oxide redox chemistry for chemical looping processes. *Nature Reviews Chemistry* **2018**, *2*, 349−364.
(13) Wang, D.; Joshi, A.; Fan, L.-S. Chemical looping technology − a manifestation of a novel fluidization and fluid-particle system for CO_2 capture and clean energy conversions. *Powder Technol.* **2022**, *409*, 117814.
(14) Qasim, M.; Ayoub, M.; Ghazali, N. A.; Aqsha, A.; Ameen, M. Recent Advances and Development of Various Oxygen Carriers for the Chemical Looping Combustion Process: A Review. *Ind. Eng. Chem. Res.* **2021**, *60*, 8621−8641.
(15) Adánez-Rubio, I.; Izquierdo, M. T.; Brorsson, J.; Mei, D.; Mattisson, T.; Adánez, J. Use of a high-entropy oxide as an oxygen carrier for chemical looping. *Energy* **2024**, *298*, 131307.
(16) Wang, X.; Gao, Y.; Krzystowczyk, E.; Iftikhar, S.; Dou, J.; Cai, R.; Wang, H.; Ruan, C.; Ye, S.; Li, F. High-throughput oxygen chemical potential engineering of perovskite oxides for chemical looping applications. *Energy Environ. Sci.* **2022**, *15*, 1512−1528.
(17) Brorsson, J.; Rehnberg, V.; Arvidsson, A. A.; Leion, H.; Mattisson, T.; Hellman, A. Discovery of Oxygen Carriers by Mining a First-Principle Database. *J. Phys. Chem. C* **2023**, *127*, 9437−9451.
(18) Gastaldi, J.; Brorsson, J.; Staničić, I.; Hellman, A.; Mattisson, T. First-Principles Estimation of Thermodynamic Properties and Phase Stability of CaMnO3−δ for Chemical-Looping Combustion. *Energy Fuels* **2025**, *39*, 9113−9120.
(19) Goldyreva, E. I.; Leonidov, I. A.; Patrakeev, M. V.; Kozhevnikov, V. L. Oxygen non-stoichiometry and defect equlibria in $CaMnO_{3-\delta}$. *J. Solid State Electrochem.* **2012**, *16*, 1187−1191.
(20) Abad, A.; Cabello, A.; Gayán, P.; García-Labiano, F.; de Diego, L.; Mendiara, T.; Adánez, J. Kinetics of $CaMn_{0.775}Ti_{0.125}Mg_{0.1}O_{2.9-\delta}$ perovskite prepared at industrial scale and its implication on the performance of chemical looping combustion of methane. *Chemical Engineering Journal* **2020**, *394*, 124863.
(21) Jiang, Q.; Zhang, H.; Deng, Y.; Kang, Q.; Hong, H.; Jin, H. Properties and reactivity of $LaCu_xNi_{1-x}O_3$ perovskites in chemical-looping combustion for mid-temperature solar-thermal energy storage. *Applied Energy* **2018**, *228*, 1506−1514.
(22) Jiang, Q.; Cao, Y.; Liu, X.; Zhang, H.; Hong, H.; Jin, H. Chemical Looping Combustion over a Lanthanum Nickel Perovskite-Type Oxygen Carrier with Facilitated O_2-Transport. *Energy Fuels* **2020**, *34*, 8732−8739.
(23) Keller, M.; Leion, H.; Mattisson, T.; Thunman, H. Investigation of Natural and Synthetic Bed Materials for Their Utilization in Chemical Looping Reforming for Tar Elimination in Biomass-Derived Gasification Gas. *Energy Fuels* **2014**, *28*, 3833−3840.
(24) Kwak, B. S.; Park, N.-K.; Baek, J.-I.; Ryu, H.-J.; Kang, M. Effect of oxidation states of Mn in $Ca_{1-x}Li_xMnO_3$ on chemical-looping combustion reactions. *Korean Journal of Chemical Engineering* **2017**, *34*, 1936−1943.
(25) Hwang, J. H.; Baek, J. I.; Ryu, H. J.; Sohn, J. M.; Lee, K.-T. Development of $MgMnO_{3-\delta}$ as an oxygen carrier material for chemical looping combustion. *Fuel* **2018**, *231*, 290−296.
(26) de Diego, L. F.; Abad, A.; Cabello, A.; Gayán, P.; García-Labiano, F.; Adánez, J. Reduction and Oxidation Kinetics of a $CaMn_{0.9}Mg_{0.1}O_{3-\delta}$ Oxygen Carrier for Chemical-Looping Combustion. *Ind. Eng. Chem. Res.* **2014**, *53*, 87−103.
(27) Thompson, W. R. On the likelihood that one unknown probability exceeds another in view of the evidence of two samples. *Biometrika* **1933**, *25*, 285−294.
(28) Deng, B.; Zhong, P.; Jun, K.; Riebesell, J.; Han, K.; Bartel, C. J.; Ceder, G. CHGNet as a pretrained universal neural network potential for charge-informed atomistic modelling. *Nature Machine Intelligence* **2023**, *5*, 1031−1041.
(29) Jain, A.; Ong, S. P.; Hautier, G.; Chen, W.; Richards, W. D.; Dacek, S.; Cholia, S.; Gunter, D.; Skinner, D.; Ceder, G.; Persson, K. A. Commentary: The Materials Project: A materials genome approach to accelerating materials innovation. *APL Materials* **2013**, *1*, No. 011002.

(30) Horton, M. K. Accelerated data-driven materials science with the Materials Project. *Nat. Mater.* **2025**, *24*, 1522.
(31) Yu, Z.; Yang, Y.; Yang, S.; Zhang, Q.; Zhao, J.; Fang, Y.; Hao, X.; Guan, G. Iron-based oxygen carriers in chemical looping conversions: A review. *Carbon Resources Conversion* **2019**, *2*, 23−34.
(32) Cho, P.; Mattisson, T.; Lyngfelt, A. Comparison of iron-, nickel-, copper- and manganese-based oxygen carriers for chemical-looping combustion. *Fuel* **2004**, *83*, 1215−1225.
(33) Abad, A.; Adánez, J.; García-Labiano, F.; de Diego, L. F.; Gayán, P.; Celaya, J. Mapping of the range of operational conditions for Cu-, Fe-, and Ni-based oxygen carriers in chemical-looping combustion. *Chem. Eng. Sci.* **2007**, *62*, 533−549. Fluidized Bed Applications.
(34) Johansson, M.; Mattisson, T.; Lyngfelt, A. Investigation of Fe_2O_3 with $MgAl_2O_4$ for Chemical-Looping Combustion. *Ind. Eng. Chem. Res.* **2004**, *43*, 6978−6987.
(35) Adánez, J.; de Diego, L. F.; García-Labiano, F.; Gayán, P.; Abad, A.; Palacios, J. M. Selection of Oxygen Carriers for Chemical-Looping Combustion. *Energy Fuels* **2004**, *18*, 371−377.
(36) Monazam, E. R.; Breault, R. W.; Siriwardane, R. Reduction of hematite (Fe_2O_3) to wüstite (FeO) by carbon monoxide (CO) for chemical looping combustion. *Chemical Engineering Journal* **2014**, *242*, 204−210.
(37) Costa, T.; Gayán, P.; Abad, A.; García-Labiano, F.; de Diego, L.; Melo, D.; Adánez, J. Mn-based oxygen carriers prepared by impregnation for Chemical Looping Combustion with diverse fuels. *Fuel Process. Technol.* **2018**, *178*, 236−250.
(38) Mei, D.; Mendiara, T.; Abad, A.; de Diego, L. F.; García-Labiano, F.; Gayán, P.; Adánez, J.; Zhao, H. Manganese Minerals as Oxygen Carriers for Chemical Looping Combustion of Coal. *Ind. Eng. Chem. Res.* **2016**, *55*, 6539−6546.
(39) Song, H.; Shah, K.; Doroodchi, E.; Wall, T.; Moghtaderi, B. Reactivity of Al_2O_3- or SiO_2-Supported Cu-, Mn-, and Co-Based Oxygen Carriers for Chemical Looping Air Separation. *Energy Fuels* **2014**, *28*, 1284−1294.
(40) Tian, X.; Su, M.; Zhao, H. Kinetics of redox reactions of CuO@TiO_2−Al_2O_3 for chemical looping combustion and chemical looping with oxygen uncoupling. *Combust. Flame* **2020**, *213*, 255−267.
(41) Zhang, Y.; Doroodchi, E.; Moghtaderi, B. Chemical looping combustion of ultra low concentration of methane with Fe_2O_3/Al_2O_3 and CuO/SiO_2. *Applied Energy* **2014**, *113*, 1916−1923.
(42) Tijani, M. M.; Aqsha, A.; Mahinpey, N. Synthesis and study of metal-based oxygen carriers (Cu, Co, Fe, Ni) and their interaction with supported metal oxides (Al_2O_3, CeO_2, TiO_2, ZrO2) in a chemical looping combustion system. *Energy* **2017**, *138*, 873−882.
(43) Alalwan, H. A.; Cwiertny, D. M.; Grassian, V. H. Co_3O_4 nanoparticles as oxygen carriers for chemical looping combustion: A materials characterization approach to understanding oxygen carrier performance. *Chemical Engineering Journal* **2017**, *319*, 279−287.
(44) Son, E. N.; Baek, S. H.; Lee, R.; Baek, J. I.; Ryu, H. J.; Yoo, D. J.; Sohn, J. M. Study on the redox characteristics of CaCo based oxygen carrier for Chemical Looping Combustion. *Chemical Engineering Journal* **2019**, *377*, 121522. ISCRE 25 Special Issue: Bridging Science and Technology.
(45) García-Labiano, F.; de Diego, L. F.; Adánez, J.; Abad, A.; Gayán, P. Temperature variations in the oxygen carrier particles during their reduction and oxidation in a chemical-looping combustion system. *Chem. Eng. Sci.* **2005**, *60*, 851−862.
(46) Adánez-Rubio, I.; Pérez-Astray, A.; Mendiara, T.; Izquierdo, M. T.; Abad, A.; Gayán, P.; de Diego, L. F.; García-Labiano, F.; Adánez, J. Chemical looping combustion of biomass: CLOU experiments with a Cu-Mn mixed oxide. *Fuel Process. Technol.* **2018**, *172*, 179−186.
(47) Cloete, S.; Giuffrida, A.; Romano, M.; Chiesa, P.; Pishahang, M.; Larring, Y. Integration of chemical looping oxygen production and chemical looping combustion in integrated gasification combined cycles. *Fuel* **2018**, *220*, 725−743.
(48) Hwang, J. H.; Son, E. N.; Lee, R.; Kim, S. H.; Baek, J. I.; Ryu, H. J.; Lee, K. T.; Sohn, J. M. A thermogravimetric study of $CoTiO_3$ as oxygen carrier for chemical looping combustion. *Catal. Today* **2018**, *303*, 13−18.
(49) Pérez-Vega, R.; Abad, A.; García-Labiano, F.; Gayán, P.; de Diego, L. F.; Izquierdo, M. T.; Adánez, J. Chemical Looping Combustion of gaseous and solid fuels with manganese-iron mixed oxide as oxygen carrier. *Energy Conversion and Management* **2018**, *159*, 221−231.
(50) Ksepko, E. Perovskite $Sr(Fe_{1-x}Cu_x)O_{3-\delta}$ materials for chemical looping combustion applications. *Int. J. Hydrogen Energy* **2018**, *43*, 9622−9634.
(51) Ksepko, E. Perovskite-type $Sr(Mn_{1-x}Ni_x)O_3$ materials and their chemical-looping oxygen transfer properties. *Int. J. Hydrogen Energy* **2014**, *39*, 8126−8137.
(52) Mihai, O.; Chen, D.; Holmen, A. Chemical looping methane partial oxidation: The effect of the crystal size and O content of $LaFeO_3$. *J. Catal.* **2012**, *293*, 175−185.
(53) Brorsson, J.; Moberg, H. K.; Hildingsson, J.; Gastaldi, J.; Mattisson, T.; Hellman, A. Material exploration through active learning − METAL. 2026; https://arxiv.org/abs/2601.03933.
(54) Wang, A.; Liang, H.; McDannald, A.; Takeuchi, I.; Kusne, A. G. Benchmarking active learning strategies for materials optimization and discovery. *Oxford Open Materials Science* **2022**, *2*, No. itac006.
(55) Muandet, K.; Fukumizu, K.; Sriperumbudur, B.; Schölkopf, B. Kernel Mean Embedding of Distributions: A Review and Beyond. *Foundations and Trends in Machine Learning* **2017**, *10*, 1−141.
(56) Bartel, C. J.; Sutton, C.; Goldsmith, B. R.; Ouyang, R.; Musgrave, C. B.; Ghiringhelli, L. M.; Scheffler, M. New tolerance factor to predict the stability of perovskite oxides and halides. *Science. Advances* **2019**, *5*, No. eaav0693.
(57) Hjorth Larsen, A.; et al. The atomic simulation environment—a Python library for working with atoms. *J. Phys.: Condens. Matter* **2017**, *29*, 273002.
(58) Togo, A.; Tanaka, I. First principles phonon calculations in materials science. *Scripta Materialia* **2015**, *108*, 1−5.
(59) Vesborg, P. C. K.; Jaramillo, T. F. Addressing the terawatt challenge: scalability in the supply of chemical elements for renewable energy. *RSC Adv.* **2012**, *2*, 7933−7947.

https://doi.org/10.1021/acsmaterialsau.5c00230
ACS Mater. Au 2026, 6, 319−326